 DOI: 10.1002/maco.201407614

The kinetics of oxygen electroreduction: A long way from iron rust to lithium–air batteries

Dedicated to Professor Dr. Martin Stratmann on the occasion of his 60th birthday

E. J. Calvo

In this communication, we review the details of the oxygen electroreduction reaction on rust layers, passive iron and well defined iron oxides as cathodes for the reaction. In particular, we highlight the important electrocatalytic role of Fe(II) sites at the surface of the oxides in contact with the aqueous electrolyte. When the same reaction takes place at bifunctional cathodes with separated metal anodes which gives rise to metal–air batteries on which much attention has been paid recently in connection with electric vehicles.

1 Introduction

It seems most appropriate for the 60th birthday celebration of Professor Dr. *Martin Stratmann* to discuss some aspects of the oxygen reduction kinetics, a topic in which we share a common interest since our first meeting at CWRU in 1983. This is also a topic to which *Martin Stratmann* has made very substantial scientific contributions.

The ubiquitous oxygen reduction reaction (ORR) [1] is very important in very different fields such as metal corrosion [2], fuel cells [3,4] and metal–air batteries [5], bio-fuel cells [6] and also the respiratory chain of biological cells [7]. Biology provides several mechanisms to activate the oxygen molecule such as through heme proteins, copper clusters and flavin containing proteins [8] while platinum based catalysts have been used for more than 50 years in fuel cell technology [9].

The electrochemical reduction of oxygen involves up to four electrons and four protons transfer steps as shown in Scheme 1 to yield water with a number of adsorbed intermediates, so it is highly catalytic. A number of theories [11–13] and experimental [3,9,14–17] approaches have been made to understand the role of oxygen reduction intermediates. In particular the role of H_2O_2 has been investigated with the rotating ring disc electrode (RRDE) and mechanistic criteria were early developed [10].

Since the start of the space race a great effort has been dedicated to fuel cells both in materials and electrocatalysis [9,18] particular the oxygen cathode with platinum and noble metal materials.

E. J. Calvo
Facultad de Ciencias Exactas y Naturales, Pabellón 2, Ciudad Universitaria, AR-1428 Buenos Aires (Argentina)
E-mail: calvo@qi.fcen.uba.ar

2 Oxygen reduction and corrosion

In corrosion the O_2 electro-reduction plays a key role as a cathode depolarizer reaction in the corrosion of metals in neutral and alkaline aerated solutions as early shown by *Traube* [19] who demonstrated the important role of oxygen in the corrosion of metals and the formation of hydrogen peroxide as a stable intermediate of the reaction.

In 1932, *Evans* proposed the "differential aeration theory" to account for the corrosion of partly immersed metals in aerated solutions [20] which consisted in the coexistence of anodic and cathodic corrosion microcells on the metal surface:

$$Fe \rightarrow Fe^{2+} + 2e \quad (1)$$

$$O_2 + 2H_2O + 4e \rightarrow 4HO^- \quad (2)$$

where the corroding metal acts as electron carrier from the anodic to the cathodic depolarization reaction.

Above pH 3 reaction (2) supersedes the discharge of protons as cathodic depolarizer [21] and in low buffered solutions where the concentration of protons is lower than the oxygen solubility (about 1 millimolar in water), the cathodic reduction of oxygen can control pH gradients at the metal electrolyte interface. It is interesting to note that weight loss measurements during the corrosion of partly immersed iron and steel have shown that the corrosion rate increases with the square root of the oxygen partial pressure, which would suggest a reaction order 0.5 in O_2 as later confirmed by our own work [22] and by others [23].

On most corroding metals the O_2 reduction takes place at potentials close to active dissolution and the electrochemical reaction occurs on oxide covered surfaces, and the process is very much slower than on platinum, gold or carbon surfaces at the same pH. It is well known that passive layers on metals inhibit the electron transfer due to their electronic properties.

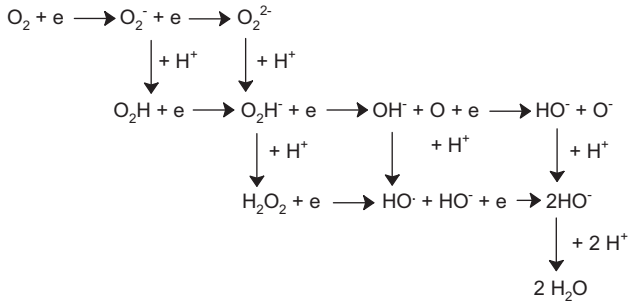

Scheme 1. Scheme of squares for the ORR with different electron and proton transfer steps

The early work of *Tarasevich* and coworkers [24] with the RRDE compared the kinetics of the oxygen electroreduction on platinum and iron in 0.1 M H_2SO_4 with production of hydrogen peroxide on Fe electrodes, as had been anticipated by *Iofa* et al. [25]. Several other RRDE studies of the ORR on iron and steel were carried out at solution pH values where the surface oxide is not stable [26] or the passivation conditions were not well defined [27,28]. These RRDE studies of the ORR were also extended to other corroding metals such as zinc [29]. *Okuyama* and *Haruyama* [30] reported the ORR on passivated Fe-18Cr alloy in borate buffer and *Babic* and *Metikoshukovic* [31] studied the ORR on stainless steel in 0.5 M NaCl.

From our own work with the ORR on passive iron in alkaline solutions [22,32,33] based on the experimental evidence of Tafel slopes, reaction orders in O_2 and HO^- and the independent study of the electrochemical reduction of hydrogen peroxide, the following mechanism for the ORR has been proposed:

$$[\mathrm{Fe(III)}]\mathrm{HO}^- + \mathrm{H_2O} + e = [\mathrm{Fe(II)OH_2}] + \mathrm{HO}^- \qquad (3)$$

Where [] represent surface iron complexes with a coordination number different from the bulk oxide. Reaction (3) explains the HO^- dependence of both the ORR and the electroreduction of H_2O_2 on passive iron in alkaline solutions; it is also consistent with capacitance-potential plots for Fe_3O_4 in EIS measurements at different HO^- activity [34]. Reaction (3) is then followed by O_2 adsorption as a μ-peroxo surface species:

$$\mathrm{O_2} + 2[\mathrm{Fe(II)OH_2}] \rightarrow [\mathrm{Fe(III)}]2\mathrm{O_2^{2-}} \qquad (4)$$

which further undergoes two one electron transfer steps, which is the rate determining step to account for the reaction order ½ in O_2 under Temkin adsorption isotherm [22]:

$$[\mathrm{Fe(III)}]2\mathrm{O_2^{2-}} + e \rightarrow [\mathrm{Fe(III)}]\mathrm{HO}^- + [\mathrm{Fe(III)}]\mathrm{HO}. \qquad (5)$$

$$[\mathrm{Fe(III)}]\mathrm{HO} + e \rightarrow [\mathrm{Fe(III)}]\mathrm{HO}^- \qquad (6)$$

At low current densities the reaction becomes insensitive to HO^- concentration which indicates that the rate of decay of surface peroxide now depends on HO^- activity as it is described by the following mechanism:

$$[\mathrm{Fe(III)}]_2\mathrm{O_2^{2-}} + \mathrm{HO}^- = [\mathrm{Fe(III)}]\mathrm{HO}^- + [\mathrm{Fe(III)}]_2\mathrm{O_2^{2-}} \qquad (7)$$

which corresponds to a change of O_2 surface coordination from μ-peroxo to end-on aduct, and then follows the peroxide disproportionation:

$$2[\mathrm{Fe(III)}]\mathrm{O_2^{2-}} + 2\mathrm{H_2O} = \mathrm{O_2} + 4\mathrm{HO}^- + 2[\mathrm{Fe(III)}] \qquad (8)$$

Evidence for peroxide disproportionation at high HO^- concentration has been obtained independently from bending of Koutecky–Levich plots due to recycling of O_2 with decrease in the apparent number of electrons exchanged by O_2 molecule [35]. Several subsequent papers from other groups confirmed these findings and mechanisms [23,36–42].

Detailed studies of the ORR on well defined iron oxides have been done in collaboration with *Stratmann* and coworkers [43,44], in particular on conducting magnetite [35,45,46] and γ-FeOOH electrodes [47]. At this point, it is worth mentioning the contribution from *Stratmann* and *Müller* [48] who studied the relation between the kinetics of oxygen reduction and the reduction of the rust layer. They concluded that O_2 is predominantly reduced within the rust scale and not at the phase boundary metal/electrolyte and that formation of Fe(II) is a condition for the ORR which is otherwise inhibited on oxidized rust layers.

A common feature of O_2 reduction on passive iron and well defined iron oxides is the occurrence of Fe(II) surface sites simultaneous to the oxygen reduction, which are needed for the specific interaction between Fe(II) and the O_2 molecules. The surface electrochemical transformations of these oxides in contact with aqueous electrolyte leading to surface Fe(III) and Fe(II) populations were studied by electrolyte electro-reflectance [34] and electrochemical impedance spectroscopy [34,43].

In these studies, it was important to establish the differences between intrinsic electron transfer properties at the oxide/electrolyte interface and the electrocatalysis for ORR of the surface oxide as a function of electrode potential, thus of surface iron speciation. The electron transfer from oxide electronic states to soluble one-electron redox species in solution, $Fe(CN)_6^{3-}$ has been studied with the rotating disc electrode. Unlike Au where the reduction of $Fe(CN)_6^{3-}$ proceeds under convective diffusion control from 0.3 V, on Fe_3O_4 and γ-FeOOH electrodes ET to soluble $Fe(CN)_6^{3-}$ is strongly inhibited where surface Fe(III) species predominate. Similar results were reported for passive iron in alkaline solution [49] and in all these cases the electronic properties of Fe(III) surfaces are responsible for the inhibited electron transfer.

A complete kinetic study of ORR on Fe_3O_4 has shown intermediate peroxide reduction (k_3), heterogeneous disproportionation (k_4), adsorption (k_6) and desorption (k_5) according to the kinetic scheme of *Wroblowa* et al. for the ORR (see Scheme 2). The kinetic analysis takes into account the chemistry of surface Fe(II). The reduction of oxygen follows an electrochemical–chemical–electrochemical (ECE) mechanism with the chemical oxidation of surface Fe(II) by O_2 and the electrochemical reduction of the Fe(III) surface site with similarities to the ORR on other Fe systems, such as passive iron in alkali and Fe-macrocycle modified electrodes.

Detailed RRDE studies of the ORR for passive iron in alkali [22] and Fe_3O_4 electrodes [46] have suggested a similar

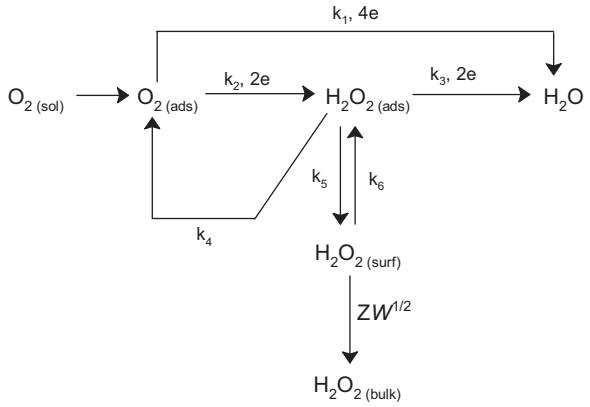

Scheme 2. ORR reduction scheme for direct and sequential paths with desorption and diffusion of H_2O_2 into solution [10]

mechanism as that proposed early by *Zagal* et al. [50] for tetrasulphonated Fe phtalocyanine modified electrodes as electrocatalysts for the ORR.

A common feature of all these systems is the formation of a surface [Fe(II)] species necessary for the adsorption of molecular oxygen and the chemical step of O_2 reaction with the ferrous surface site acting as a redox mediator in the oxygen molecule activation. However the ORR takes place with a higher overpotential than on iron macrocycles adsorbed on carbon electrodes due to the shift in the Fe(III)/Fe(II) redox couple potential due to the higher reorganization energy for the oxide surface iron complex as compared to the iron phtalocyanines or porphyrins.

Stratmann has made an important contribution to the understanding the mechanisms of atmospheric corrosion by oxygen from the air. In the presence of oxygen and water, rust is formed on iron and ferrous alloys according to:

$$4Fe + 3O_2 + 2H_2O \rightarrow 4FeOOH \quad (9)$$

An aqueous layer on the surface (electrolyte) is formed by water condensation. As ambient temperature changes during the day evaporation causes wet and dry periods to alternate.

A model for the atmospheric corrosion was proposed by *Evans* and *Taylor* [2] and then experimentally investigated by *Stratmann* et al. using a variety of techniques [51–55] Therefore the reactions taking place in the alternating wet–dry cycles are different: During the first stage (wet period), the anodic dissolution of iron is mainly balanced by the reduction of Fe(III) species within the rust layer and very little oxygen is reduced on γ-FeOOH as expected due to the low solubility of O_2 and the slow ORR electrocatalysis on the poorly conducting oxide surface. Direct access of O_2 to the underlying metal is limited to nanometer diameter. Porous ferric species in the rust layer act as cathodic depolarizers with faster kinetics than molecular oxygen.

The electrons produced in the metal dissolution are consumed by reduction of γ-FeOOH in the layer since ORR is a slow process under those conditions.

$$\gamma - FeOOH + H^+ + e \rightarrow \gamma - Fe.OH.OH \quad (10)$$

Stratmann has demonstrated that lepidocrocyte (γ-FeOOH) keeps its crystal structure while being reduced to yield a more electronic and ionic conducting oxide but if the doping level of Fe(II) in the lattice exceeds 2–4% then Fe_3O_4 (magnetite) begins to form irreversibly and upon oxidation magnetite yields maghemite (γ-Fe_2O_3) [53]. After drying the thin electrolyte layer, in the dry period, the corrosion rate decreases and the dry porous structure allows oxygen to penetrate the rust layer and to re-oxidize the ferrous sites back to the ferric state. Thus in this part of the wet–dry cycle oxidizing power is stored in the rust layer as in a battery. So, unlike passivated iron and iron oxides in contact with aqueous electrolyte where molecular oxygen is the cathodic depolarizer in atmospheric corrosion oxygen depolarization is indirect through the formation of Fe(III) oxides on the metal surface.

3 Oxygen reduction and batteries

While metal corrosion in air is almost a short circuit process with electrons flowing from anodic to cathodic sites in the corroding metal or rust layer, the same reactions can generate electricity in metal–air batteries by redox processes in separate electrodes: The metal dissolves at the anode while atmospheric oxygen electroreduction takes place at the cathode during discharge of the battery thus obtaining electrical work. Several metal–air systems, Zn–O_2, Mg–O_2, Al–O_2, Li–O_2, have been used in primary batteries [5]. The Zn–air battery has been used for years in hearing aids and military applications.

Metal–air batteries can be compared to fuel cells where the metal dissolution replaces the fuel in the anode, and exhibit notable higher theoretical energy density than other conventional batteries since O_2 from the air is not stored in the battery. However, during discharge a mass increase occurs due to the incorporation of oxygen atoms in the reaction product metal oxide.

Since Li is the lightest metal, Li–air battery with a gravimetric energy density of 11 700 Wh/kg (Li_2O) or 5280 Wh/kg (LiO_2) comparable to fossil fuels such as gasoline has been considered an alternative for electric vehicles, however there are still great technically challenges to develop electrically rechargeable metal–air batteries. Metal batteries (Zn, Mg, Al) may also be recharged mechanically in electric vehicles by replacing the discharged metal anode and spent electrolyte by a fresh metal cartridge while reprocessing and recycling the used anode and electrolyte.

Interestingly, the Fe–O_2 corrosion reaction has been suggested recently in a low cost ($100/kWh) and environmentally friendly metal–air battery given the abundant availability of iron [56–58]. The overall cell reaction in this case is:

$$Fe + 1/2O_2 + H_2O = Fe(OH)_2 \quad (11)$$

During discharge the reaction proceeds in alkali from left to right while the back reaction takes place during charging. The open circuit potential is about 1.28 V and the theoretical energy density is 764 Wh/Kg. The discharge anodic and cathodic processes are identical to the iron corrosion reactions described above, however in the battery they take place on separate

electrodes: iron anode and bifunctional oxygen cathode, respectively. Further discharge of the battery beyond two-electron step will lead to the formation of iron oxyhydroxide or magnetite and the reversibility of the battery is handicapped. Furthermore, the Faradaic efficiency is limited to less than 50% due to the simultaneous discharge of hydrogen on the iron electrode during charging and additives have been investigated to inhibit the hydrogen reaction.

High energy density rechargeable lithium–air battery has attracted much attention in recent time for applications in electric vehicles since the present lithium-ion battery technology is insufficient for the long term demands of transport and cannot provide a driving range over 100 miles between charges [59–62]. Aqueous and non-aqueous Li–air batteries have been described, but in the former case the anode needs to be protected because lithium reacts violently with water. In the non-aqueous Li–air battery introduced in 1996 by *Abraham* [59], during discharge a Li anode dissolves in non-aqueous electrolyte and the resulting Li^+ ions react with O_2 reduction products to form insoluble lithium peroxide Li_2O_2 at a porous carbon cathode. *Bruce* and coworkers [63] demonstrated that the electrochemical reaction of Li^+ with oxygen to yield insoluble Li_2O_2 in non-aqueous electrolyte is reversible sustaining more than several charge/discharge cycles.

It has also been shown that the electrode kinetics of the ORR in lithium air battery cathodes strongly depends on the solvent [64,65], electrolyte cation [66] and electrode material. In non-aqueous solutions containing tetra alkylammonium cations the reversible one-electron reduction product, superoxide is stable but in Li^+ containing electrolyte the reaction products LiO_2 and Li_2O_2 are insoluble and therefore the reaction is irreversible with surface passivation. Further-more, O_2^- can attack nucleophillically most aprotic solvents employed [60,67,68] as in situ infrared experiments and mass spectrometry have suggested [65,69–71] and the kinetics of the attack on propylene carbonate have been quantified with the RRDE by measuring the ring current transient response to a potential step at the disc electrode [72].

Among non-aqueous solvents, DMSO with a very large dipolar moment ($\mu = 4{,}3$ D) and the appropriate Li^+ coordination geometry has been used in Li–O_2 cathodes [64,73,74]. *Peng* et al. [75] have shown that in this electrolyte and using a porous gold electrode the Li–air battery can be recharged with 95% capacity retention in 100 cycles.

One of the major challenges for the non-aqueous Li–O_2 battery is the efficient oxidation of solid Li_2O_2 in the porous cathode during battery charging. On recharging the Li–air battery a large overpotential, i.e. >4 V, is needed to oxidize solid Li_2O_2 into O_2 and Li^+ [76]. At such high potentials DMSO is electrochemically oxidized to dimethyl sulfone on Au above 4.2 V as has been demonstrated recently by in situ infrared subtractively normalized interfacial Fourier transform infrared spectroscopy (SNIFTIRS) experiments [77].

We have also investigated the morphology of oxygen reduction insoluble products in DMSO $LiPF_6$ electrolyte by ex situ AFM on HOPG after treatment at different electrode potentials for the oxygen reduction (discharge) and O_2 evolution by Li_2O_2 oxidation (charge) [78]. Decoration of step edges is apparent and also deposits at basal plane terraces grow by peroxide aggregation. Re-oxidation of Li_2O_2 and thus recovery of the HOPG surface does not take place until very positive potentials are reached where DMSO is electrochemically oxidized to dimethyl sulfone.

The peculiar Li^+ solvation capacity of DMSO has been recently reported and soluble superoxide radical anion has been detected with the RRDE in acetonitrile $LiClO_4$ solutions containing only 0.1 M DMSO, unlike pure acetonitrile lithium electrolytes with no evidence of soluble O_2^- at all [79].

In highly donor DMSO (Gutmann donor number 29.8) and the highest dipole moment, 3.96 D with the appropriate geometry to coordinate Li^+ ions (solvated by four DMSO molecules) would form a non-contact ion pair with superoxide ions precluding the disportionation reaction in solution. In acetonitrile solutions, on the other hand, the solvent ion interaction is weak and thus the lithium superoxide species are very unstable and disproportionte into Li_2O_2 and O_2 with no soluble superoxide detection. Conversely, adsorbed ion pairs $[O_2^-]_{ads}[Li^+]_{ads}$ can readily disproportionate due to the easy shuttling of electrons at the electrode surface which otherwise requires a bimolecular encounter in the bulk solution while on the surface it is not necessary for two adsorbed superoxide molecules to be adjacent due to the fast mobility of surface electrons. As shown in Scheme 3, the solvated non-contact ion pair $[O_2^-]_{DMSO}[Li^+]_{DMSO}$ can diffuse out in solution and be detected at the ring electrode while the adsorbed contact ion pair readily decomposes.

The stronger solvation of Li^+ in DMSO with respect to CH_3CN stabilizes solvated Li–O_2^- ion pairs as shown by molecular dynamic simulations [80]. and is also reflected in the Li/Li^+ higher electrode potential in DMSO (3.7 V in 0.1 M $LiPF_6$ in DMSO and 3.23 V in 0.1 M $LiPF_6$ in acetonitrile with respect to a Ag/Ag^+, 10 m $AgNO_3$, 0.1 M $TBAPF_6$ reference electrode).

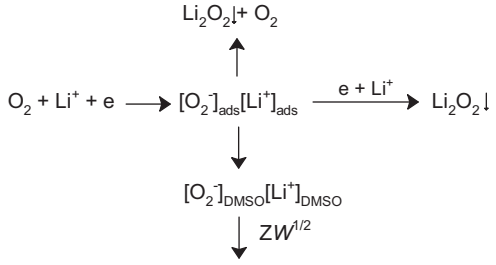

Scheme 3. Scheme for the ORR in Li^+ containing DMSO electrolyte

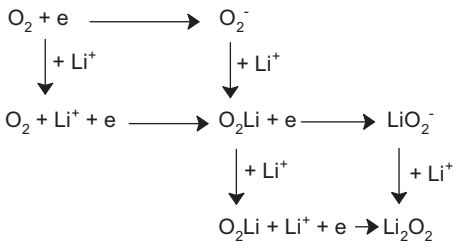

Scheme 4. Scheme of squares for the ORR in L^{i+} containing aprotic electrolyte

For metal corrosion, fuel cells and metal–air batteries where the ORR plays a key role, it is interesting to compare the roles of H^+ and Li^+ ions in stabilizing the ORR intermediates in the schemes of squares Scheme 1 and Scheme 4 which define the minimum free energy reaction pathway and therefore the mechanisms.

4 References

[1] J. P. Hoare, *The Electrochemistry of Oxygen*, Interscience, New York **1968**.
[2] U. R. Evans, C. A. J. Taylor, *Corros. Sci.* **1972**, *12*, 227.
[3] N. Ramaswamy, S. Mukerjee, *Adv. Phys. Chem.* **2012**, *2012*, 491604.
[4] N. M. Markovic, T. J. Schmidt, V. Stamenkovic, P. N. Ross, *Fuel Cells* **2001**, *1*, 105.
[5] F. Cheng, J. Chen, *Chem. Soc. Rev.* **2012**, *41*, 2172.
[6] P. Scodeller, R. Carballo, R. Szamocki, L. Levin, F. Forchiassin, E. J. Calvo, *JACS* **2010**, *132*, 11132.
[7] A. Boveris, B. Chance, *Biochem. J.* **1973**, *134*, 707.
[8] W. B. Tolman, E. I. Solomon, *Inorg. Chem.* **2010**, *49*, 3555.
[9] K. Kinoshita, *Electrochemical Oxygen Technology*, Wiley, New York **1992**.
[10] P. Vassilev, M. T. M. Koper, *J. Phys. Chem. C* **2007**, *111*, 2607.
[11] J. K. Norskov, J. Rossmeisl, A. Logadottir, L. Lindqvist, J. R. Kitchin, T. Bligaard, H. Jonsson, *J. Phys. Chem. B* **2004**, *108*, 17886.
[12] C. H. Kjaergaard, J. Rossmeisl, J. K. Norskov, *Inorg. Chem.* **2010**, *49*, 3567.
[13] V. R. Stamenkovic, B. Fowler, B. S. Mun, G. Wang, P. N. Ross, C. A. Lucas, N. M. Markovic, *Science* **2007**, *315*, 493.
[14] S. Nayak, P. U. Biedermann, M. Stratmann, A. Erbe, *Electrochim. Acta* **2013**, *106*, 472.
[15] S. Nayak, P. U. Biedermann, M. Stratmann, A. Erbe, *Phys. Chem. Chem. Phys.* **2013**, *15*, 5771.
[16] I. Katsounaros, W. B. Schneider, J. C. Meier, U. Benedikt, P. U. Biedermann, A. Cuesta, A. A. Auer, K. J. J. Mayrhofer, *Phys. Chem. Chem. Phys.* **2013**,*15*, 8058.
[17] H. S. Wroblowa, Y. C. Pan, G. Razumney, *J. Electroanal. Chem.* **1976**, *69*, 195.
[18] A. A. Gewirth, M. S. Thorum, *Inorg. Chem.* **2010**, *49*, 3557.
[19] M. Traube, *Ann. Chem.* **1882**, 815.
[20] U. R. Evans, T. P. Hoar, *Proc. R. Soc. Ser. A* **1932**, *137*, 343.
[21] P. Lorbeer, W. J. Lorenz, *Electrochim. Acta* **1980**, *25*, 375.
[22] E. J. Calvo, D. J. Schiffrin, *J. Electroanal. Chem.* **1988**, *243*, 171.
[23] S. Zecevic, D. M. Drazic, S. Gojkovic, *J. Electroanal. Chem.* **1989**, *265*, 179.
[24] M. A. Marinich, L. I. Antropov, M. R. Tarasevich, *Ukr. Khim. Zh.* **1978**, *44*, 357.
[25] Z. A. Iofa, M. A. Makhbuba, *Zashchita Metallov (Translated into English)* **1967**, *3*, 329.
[26] V. Jovancicevic, J. O. Bockris, *J. Electrochem. Soc.* **1986**, *133*, 1797.
[27] H. S. Wroblowa, S. B. Qaderi, *J. Electroanal. Chem.* **1990**, *279*, 231.
[28] H. S. Wroblowa, *J. Electroanal. Chem.* **1992**, *339*, 31.
[29] H. S. Wroblowa, S. B. Qaderi, *J. Electroanal. Chem.* **1990**, *295*, 153.
[30] M. Okuyama, S. Haruyama, *Corros. Sci.* **1990**, *31*, 521.
[31] R. Babic, M. Metikoshukovic, *J. Appl. Electrochem.* **1993**, *23*, 352.
[32] E. J. Calvo, *J. Electrochem. Soc.* **1983**, *130*, C334.
[33] E. J. Calvo, D. J. Schiffrin, *J. Electroanal. Chem.* **1984**, *163*, 257.
[34] P. A. Castro, E. R. Vago, E. J. Calvo, *J. Chem. Soc. Faraday Trans.* **1996**, *92*, 3371.
[35] E. R. Vago, E. J. Calvo, *J. Electroanal. Chem.* **1995**, *388*, 161.
[36] S. Zecevic, D. M. Drazic, S. Gojkovic, *Electrochim. Acta* **1991**, *36*, 5.
[37] S. L. Gojkovic, S. K. Zecevic, D. M. Drazic, *Electrochim. Acta* **1994**, *39*, 975.
[38] S. L. Gojkovic, S. K. Zecevic, M. D. Obradovic, D. M. Drazic, *Corros. Sci.* **1998**, *40*, 849.
[39] S. Zecevic, D. M. Drazic, S. Gojkovic, *Corros. Sci.* **1991**, *32*, 563.
[40] S. L. Gojkovic, S. K. Zecevic, D. M. Drazic, *Electrochim. Acta* **1992**, *37*, 1845.
[41] D. M. Drazic, S. Gojkovic, S. K. Zecevic, V. Radmilovic, *Corros. Sci.* **1992**, *33*, 791.
[42] S. L. Gojkovic, S. K. Zecevic, D. M. Drazic, *J. Electroanal. Chem.* **1995**, *399*, 127.
[43] E. R. Vago, E. J. Calvo, M. Stratmann, *Electrochim. Acta* **1994**, *39*, 1655.
[44] E. R. Vago, K. Deweldige, M. Rohwerder, M. Stratmann, *Fresenius J. Anal. Chem.* **1995**, *353*, 316.
[45] E. R. Vago, E. J. Calvo, *J. Electroanal. Chem.* **1992**, *339*, 41.
[46] E. R. Vago, E. J. Calvo, *J. Chem. Soc. Faraday Trans.* **1995**, *91*, 2323.
[47] E. R. Vago, *Doctoral Thesis*, University of Buenos Aires, FCEyN **1993**.
[48] M. Stratmann, J. Müller, *Corros. Sci.* **1994**, *36*, 327.
[49] A. M. T. Olmedo, R. Pereiro, D. J. Schiffrin, *J. Electroanal. Chem.* **1976**, *74*, 19.
[50] J. Zagal, P. Bindra, E. Yeager, *J. Electrochem. Soc.* **1980**, *127*, 1506.
[51] M. Stratmann, K. Bohnenkamp, H. J. Engell, *Werkstoffe und Korrosion – Mater. Corros.* **1983**, *34*, 604.
[52] M. Stratmann, K. Bohnenkamp, H. J. Engell, *Corros. Sci.* **1983**, *23*, 969.
[53] M. Stratmann, *Corros. Sci.* **1987**, *27*, 869.
[54] M. Stratmann, H. Streckel, *Corros. Sci.* **1990**, *30*, 681.
[55] M. Stratmann, H. Streckel, *Corros. Sci.* **1990**, *30*, 697.
[56] A. K. Manohar, S. Malkhandi, B. Yang, C. Yang, G. K. S. Prakash, S. R. Narayanan, *J. Electrochem. Soc.* **2012**, *159*, A1209.
[57] A. K. Manohar, C. Yang, S. Malkhandi, G. K. S. Prakash, S. R. Narayanan, *J. Electrochem. Soc.* **2012**, *160*, A2078.
[58] S. R. Narayanan, G. K. S. Prakash, A. Manohar, B. Yang, S. Malkhandi, A. Kindler, *Solid State Ionics* **2012**, *216*, 105.
[59] K. M. Abraham, in: K. M. A. Bruno Scrosati, W. A. van Schalkwijk, J. Hassoun (Eds.), *Lithium Batteries: Advanced Technologies and Applications*, John Wiley & Sons, Inc., New York **2013**.
[60] P. G. Bruce, S. A. Freunberger, L. J. Hardwick, J.-M. Tarascon, *Nat. Mater.* **2012**,*19*, 11.
[61] J. Christensen, P. Albertus, R. S. Sanchez-Carrera, T. Lohmann, B. Kozinsky, R. Liedtke, J. Ahmed, A. Kojic, *J. Electrochem. Soc.* **2012**, *159*, R1.
[62] L. J. Hardwick, P. G. Bruce, *Curr. Opin. Solid State Mater. Sci.* **2012**, *16*, 178.

[63] T. Ogasawara, A. Debart, M. Holzapfel, P. Novak, P. G. Bruce, *J. Am. Chem. Soc.* **2006**, *128*, 1390.
[64] C. O. Laoire, S. Mukerjee, K. M. Abraham, E. J. Plichta, M. A. Hendrickson, *J. Phys. Chem. C* **2010**, *114*, 9178.
[65] B. D. McCloskey, D. S. Bethune, R. M. Shelby, G. Girishkumar, A. C. Luntz, *J. Phys. Chem. Lett.* **2011**, *2*, 1161.
[66] C. O. Laoire, S. Mukerjee, K. M. Abraham, E. J. Plichta, M. A. Hendrickson, *J. Phys. Chem. C* **2009**, *113*, 20127.
[67] Y. Chen, S. A. Freunberger, Z. Peng, F. Barde, P. G. Bruce, *J. Am. Chem. Soc.* **2012**, *134*, 7952.
[68] S. A. Freunberger, Y. Chen, N. E. Drewett, L. J. Hardwick, F. Barde, P. G. Bruce, *Angew. Chem. Int. Ed.* **2011**, *50*, 8609.
[69] B. D. McCloskey, R. Scheffler, A. Speidel, G. Girishkumar, A. C. Luntz, *J. Phys. Chem. C* **2012**, *116*, 23897.
[70] B. D. McCloskey, D. S. Bethune, R. M. Shelby, T. Mori, R. Scheffler, A. Speidel, M. Sherwood, A. C. Luntz, *J. Phys. Chem. Lett.* **2012**, *3*, 3043.
[71] B. D. McCloskey, A. Speidel, R. Scheffler, D. C. Miller, V. Viswanathan, J. S. Hummelshoj, J. K. Norskov, A. C. Luntz, *J. Phys. Chem. Lett.* **2012**, *3*, 997.
[72] J. Herranz, A. Garsuch, H. A. Gasteiger, *J. Phys. Chem. C* **2012**, *116*, 19084.
[73] D. Xu, Z.-L. Wang, J.-J. Xu, L.-L. Zhang, X.-B. Zhang, *Chem. Commun.* **2012**, *48*, 6948.
[74] M. J. Trahan, S. Mukerjee, E. J. Plichta, M. A. Hendrickson, K. M. Abraham, *J. Electrochem. Soc.* **2013**, *160*, A259.
[75] Z. Peng, S. A. Freunberger, Y. Chen, P. G. Bruce, *Science* **2012**, *337*, 563.
[76] B. M. Gallant, D. G. Kwabi, R. R. Mitchell, J. Zhou, C. V. Thompson, Y. Shao-Horn, *Energy Environ. Sci.* **2013**, *6*, 2518.
[77] N. Mozhuzhukina, L. Mendez De Leo, P. E. J. Calvo, *J. Phys. Chem. C* **2013**, *117*, 18375.
[78] S. E. Herrera, A. Y. Tesio, R. Clarenc, E. J. Calvo, *Phys. Chem. Chem. Phys.* **2014**, DOI: 10.1039/C3CP54621G.
[79] E. J. Calvo, N. Mozhzhukhina, *Electrochem. Commun.* **2013**, *31*, 56.
[80] N. Mozhzhukhinaa, R. Semino, G. Zaldivar, D. H. Lariaa, E. J. Calvo, **2013**, in preparation.

(Received: January 15, 2014) W7614
(Accepted: January 15, 2014)

